Nanoscale Advances

PAPER

View Article Online
View Journal | View Issue

Cite this: *Nanoscale Adv.*, 2019, **1**, 1571

Programmed supramolecular nanoassemblies: enhanced serum stability and cell specific triggered release of anti-cancer drugs†

Sanchaita Mondal,[a] Moumita Saha,[b] Mousumi Ghosh,[a] Subrata Santra,[a] Mijan A. Khan,[a] Krishna Das Saha*[b] and Mijanur R. Molla *[a]

A bolaamphiphilic cross-linked nanoassembly endowed with pH responsive degradation features has been designed and fabricated for stable noncovalent guest encapsulation and controlled release. The self-assembled bolaamphiphile is utilized to prepare cross-linked nanoassemblies to further stabilize the noncovalent guest encapsulation at a concentration below its critical aggregation concentration (CAC) in a large volume of water or serum for drug delivery applications. Thus, this system can simultaneously address premature drug release and safety issues. The nanoassemblies integrated with a β-thioester linker, which can be hydrolyzed selectively under mildly acidic conditions (pH ∼ 5.3) at a slow rate, thus enable controlled release of guest molecules. Biological evaluation revealed that doxorubicin loaded cross-linked nanoassemblies (CNs–DOX) are nontoxic to normal cells such as HEK-293 or PBMC, but in contrast, showed a robust apoptotic effect on colon cancer cells, HCT-116, indicating excellent specificity. Thus, the fabrication reproducibility, robust stability, triggered drug release and cell selective toxicity behavior make this small molecular system very promising in the field of chemotherapeutic applications.

Received 27th January 2019
Accepted 29th January 2019

DOI: 10.1039/c9na00052f

rsc.li/nanoscale-advances

Introduction

Programmed supramolecular nanoassemblies, which undergo disassembly in response to a particular stimulus, have been of great interest owing to their potential biomedical applications[1–4] especially in the fields of drug delivery and gene transfection.[5–9] Although stimuli-responsive polymers have widely been used as promising drug delivery materials in nanomedicine,[10–13] they have some inherent defects including metastability, lack of homogeneity, poor reproducibility of the same molecular weight and polydispersity, which have to be addressed for successful clinical evaluation. On the other hand, dendrimers and amphiphilic or bolaamphiphilic small molecules have quantitative reproducibility of the same molecular weight and a high degree of control over their polydispersity and size.[14–20] Hence, it is interesting to study the self-assembly and disassembly characteristics of these molecules integrated with a stimuli-responsive functional group.[21–30] In dendrimers, the major problems are insolubility and non-degradability, whereas in small molecule-based assemblies, the major drawbacks are high critical aggregation concentrations (CAC) and low inherent stabilities. Although polymer and dendrimer-based assemblies have low CAC, it is very challenging to maintain the stability of the nanoassemblies like micelles,[23,31–35] vesicles[24,36–39] and liposomes[40–43] made of polymers, dendrimers or small molecules in the vascular system. Due to the dilution effect in a large volume of blood serum, nanoassemblies disassemble and eventually release guest molecules in undesired locations. Hence, the fabrication of alternative nanoassemblies, which have polymeric micelle-like features and will overcome the challenges mentioned above, would be highly beneficial.

Here, we propose that if the stability issues are taken care of, small molecule-based nanoassemblies might become a promising candidate in the field of drug delivery. To eliminate the dilution effect and enhance the stability, the advantageous approach is cross-linking either the core or the surface of the self-assembled particles. The cross-linking will minimize the leaking of encapsulated guest molecules, increase the stability of nanoassemblies and eliminate the possibility of premature guest release. To the best of our knowledge, there are only a few reports in the literature regarding small molecule[44–46] based cross-linked nanoparticles compared to polymer-based systems.[47–54] Hence, we wanted to explore this area to establish a small molecule-based robust drug delivery platform. To this end, we have synthesized a bolaamphiphilic small molecule integrated with a β-thioester linker, which is known to slowly hydrolyze selectively under mild acidic conditions (pH ∼

[a]University of Calcutta, Department of Chemistry, 92 APC Road, Kolkata-700009, India. E-mail: mrmchem@caluniv.ac.in

[b]Cancer Biology and Inflammatory Disorder Division, Indian Institute of Chemical Biology, 4, Raja S C Mullick Road, Kolkata-700032, India

† Electronic supplementary information (ESI) available. See DOI: 10.1039/c9na00052f

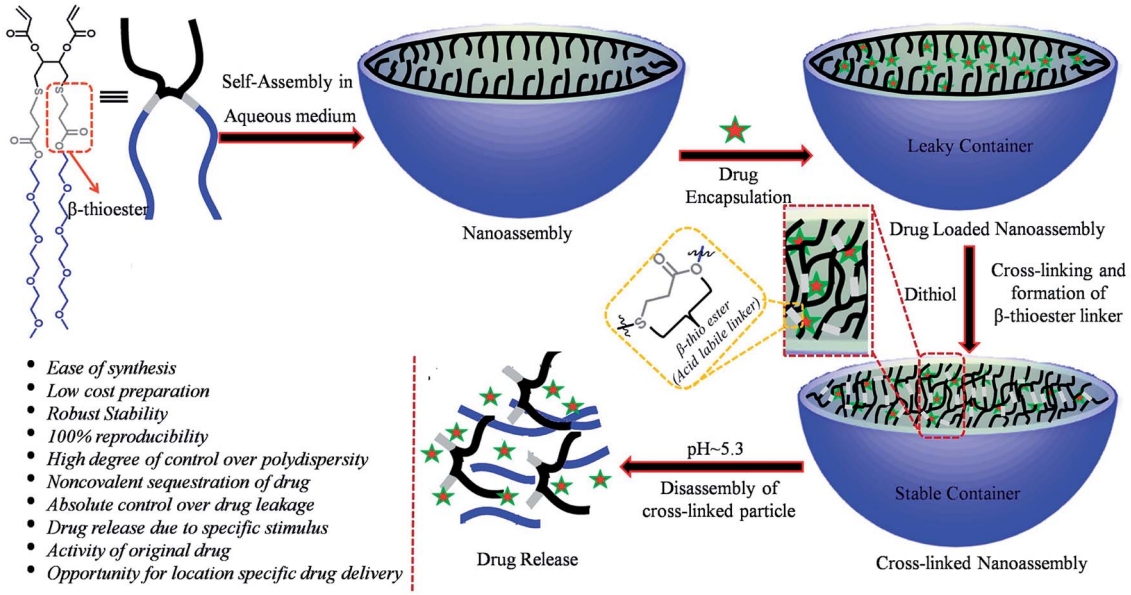

Scheme 1 Schematic representation of the nanoassembly formation, cross-linking and triggered disassembly of the bolaamphiphilic nanoassembly.

5.3)[31,38,51,55,56] unlike other acid-labile functional groups such as acetal, ketal, hydrazone and orthoester, which hydrolyze very rapidly, and result in the burst release of encapsulated guest molecules.[57–62] The feature of the β-thioester group has previously been utilized for various purposes such as for controlled drug delivery or lysosomal protein delivery, but the number of reports is very low.[31,38,50] Therefore, this fact motivated us to design a novel molecule with β-thioester to achieve pH responsive noncovalent guest release in a sustained manner. Herein, we have shown the synthesis of a bolaamphiphilic small molecule, the formation of nanoassemblies in an aqueous milieu and cross-linking of its core by the Michael addition reaction, which creates multiple copies of the β-thioester linker in the core of the micellar assemblies (Scheme 1). Furthermore, we show pH-responsive sustained guest release, the stability of the cross-linked nanoassemblies (CNs) in blood serum and finally, *in vitro* anti-cancer drug delivery applications. The CNs–DOX was found to display benign nature to normal cells, but toxicity to cancer cells, which makes it a potential candidate in therapeutic applications.

Experimental

Synthesis and characterization

The detailed synthetic scheme of the bolaamphiphile, protocol and characterization data are provided in the ESI.†

Determination of critical aggregation concentration (CAC)

At first, a measured amount of a solution of Nile red in acetone (100 μL, 0.1 mM) was placed in various screw-capped vials and the solvent was evaporated. Solutions of various concentrations (1 mM, 0.8 mM, 0.6 mM, 0.4 mM, 0.2 mM, 0.08 mM *etc.*) of BA were added to the vials that contained Nile red and the mixture was sonicated and allowed to stand for 2 h before fluorescence spectroscopic analysis (λ_{ex} = 530 nm). The final concentration of Nile red was 10^{-5} M. The emission intensity of the encapsulated Nile red at 585 nm was plotted *versus* the concentration of BA and the inflection point of such a plot was taken as the CAC of BA.

Fabrication of cross-linked nanoassemblies (CNs)

Hexylamine (0.065 μL, 0.0005 mmol in 500 μL acetone) and hexanedithiol (0.3 μL, 0.002 mmol in 500 μL acetone) were added simultaneously to a 2 mL solution of BA (1 mM). Then the mixture was stirred for 48 h and filtered with a 0.45 μm syringe filter.

Atomic force microscopy (AFM)

5 μL of the samples (1 mM) were deposited onto a freshly cleaved muscovite Ruby mica sheet (ASTM V1 Grade Ruby Mica from MICAFAB, Chennai) for 5–10 minutes, and then the sample was dried by using a vacuum dryer. AAC mode AFM was performed using a Pico plus 5500 AFM (Agilent Technologies USA) with a piezo scanner with a maximum range of 9 μm. Micro-fabricated silicon cantilevers of 225 μm in length with a nominal spring force constant of 21–98 N m^{-1} from Nano sensors were used. Cantilever oscillation frequency was tuned into resonance frequency. The cantilever resonance frequency was 150–300 kHz. The images (256 by 256 pixels) were captured with a scan size between 0.5 and 5 μm at a scan rate of 0.5 lines per s. The images were processed by flatten using Pico view1.4 version software (Agilent Technologies, USA). Image manipulation was done through Pico Image Advanced version software (Agilent Technologies, USA).

Transmission electron microscopy (TEM)

A solution of the sample in water (20 μL, 1 mM) was placed on a TEM grid (300-mesh carbon-coated Cu grid). The samples were allowed to dry in air at room temperature for a few hours before the measurements were recorded.

Dynamic light scattering (DLS)

For the DLS measurements, 1 mM of BA and cross-linked BA was used. The measurements were carried out at room temperature.

Stability test

The cross-linked nanoassemblies were diluted to a concentration below the CAC and the size change was recorded using DLS. Both cross-linked and uncross-linked nanoassemblies were diluted with FBS and the size change was examined every 2 h by using DLS.

pH responsive degradation

The cross-linked nanoassemblies were treated with Tris buffer of pH 5.3 and pH 7.4 separately. The time dependent DLS spectra were measured to check the size change over time.

Pyrene encapsulation and pH responsive release

10 μL of pyrene stock solution (10^{-3} M) in acetone was transferred to a vial and solvent was removed by blowing air to make a thin film. To this, a solution of BA (2 mL, 1 mM) was added, stirred for 5 minutes and sonicated for 5 minutes. Then the solution was allowed to stand for 2 h at room temperature to get a homogeneous solution. This dye encapsulated solution was used for fluorescence spectra measurement to check the extent of dye encapsulation. After the confirmation of pyrene encapsulation, the core of the nanoassemblies was cross-linked using dithiol by the Michael addition reaction. For the pH responsive release study, the pH of the pyrene encapsulated solutions (both cross-linked and uncross-linked) was adjusted to pH 5.3 and pH 7.4 using Tris buffer. Then time dependent UV-Vis spectra were recorded to examine the pyrene release.

Doxorubicin encapsulation

A measured amount (1.12 mg) of hydrophobic DOX was added to a solution of BA (2 mL, 1 mM) followed by vortexing for 10 minutes and sonication for 2 minutes. A red color emulsion was formed which was filtered through a 0.45 μm of syringe filter. To obtain DOX-encapsulated cross-linked nanoassemblies (CNs–DOX), it was then cross-linked following the above-mentioned procedure.

pH responsive release of doxorubicin

The pH-responsive DOX release from DOX loaded cross-linked and uncross-linked nanoassemblies (CNs–DOX and UCNs–DOX) was evaluated by equilibrium dialysis using a 1000 MWCO dialysis bag at pH 5.3 and pH 7.4 (Tris buffer). Each 500 μL of the aliquot sample of CNS–DOX or UCNs–DOX (conc. = 2.0 mg mL^{-1}) was added into a dialysis bag (1000 MWCO) and dialyzed against 15.0 mL of different buffers (Tris buffer of pH 5.3 and 7.4). At predetermined time periods, 1.0 mL of the solution was collected from the corresponding different reservoirs and the released DOX was detected by using fluorescence spectra. To keep a constant volume after each sampling, the measured sample solution was added back to the reservoir.

Biological studies

Reagents. Dulbecco's Modified Eagle's Medium (DMEM), Fetal Bovine Serum (FBS), penicillin, streptomycin, neomycin (PSN) antibiotic, ethylenediamine tetra acetic acid (EDTA) and trypsin were bought from Gibco BRL (Grand Island, NY, USA). 3-(4,5-Dimethylthiazol-2-yl)-2,5-diphenyltetrazolium bromide (45989, MTT-CAS 298-93-1-Calbiochem) and DMSO were bought from Merck-Millipore. Tissue culture plastic wares were bought from Genetix Biotech Asia Pvt. Ltd. Blood for PBMC isolation was collected from a healthy human volunteer. The cell lines HEK293 and HCT116 were purchased from the National Centre for Cell Science (NCCS), an Autonomous Institute of Dept. of Biotechnology, Govt. of India.

Ethical statement. All the biological experiments were performed in accordance with the guidelines and approval of the Institutional Human Ethics Committee and Biosafety Committee at the CSIR-Indian Institute of Chemical Biology, Kolkata, India. Informed written consent was obtained from the human volunteer.

Cell culture. The HCT116 and HEK293 cells were cultured in DMEM mixed with 10% FBS and 1% antibiotic (PSN) at 37 °C in a humidified incubator with 5% CO_2. The cells were harvested with 0.5% trypsin and seeded at a required density to allow them to re-equilibrate a day before the start of the experiment.

Isolation of PBMC. 2 mL blood was collected in a 15 mL tube using the anticoagulant EDTA. The blood was diluted 2× with PBS (phosphate buffered saline) + 2% FBS (fetal bovine serum). In another tube 10 mL Ficoll-paque was taken and the diluted blood solution was added slowly on top of the Ficoll solution. This mixture was centrifuged at room temperature for 30 min at 400 × *g*. After that the upper plasma layer was discarded without disturbing the remaining plasma-Ficoll interface solution where the lymphocytes were found. Then the lymphocyte cell layer was separated from the plasma-Ficoll interface in another 15 mL tube and then it was further diluted 3× with PBS and centrifuged at room temperature for 10–15 min at 200 × *g*. After discarding the PBS, the cell pellet was suspended in RPMI 1640 medium and cultured at 37 °C in a humidified incubator with 5% CO_2.

Cytotoxicity assay. Cell toxicity was detected by the MTT assay. The HCT 116, HEK-293 and PBMC cells (1×10^6 cells per well) were seeded in a 96-well plate. Then, different concentrations of CNs, UCNs, CNs–DOX, UCNs–DOX and free DOX were added to the cell medium and incubated for 24 h. After 24 h of incubation, the medium was changed to 20 μL of MTT solution (4 mg mL^{-1}) and incubated again for 3 h. Next, a measured volume of DMSO (100 μL) was added to each well and the cell cytotoxicity was measured using a microplate reader at 595 nm wavelength.

Cellular uptake study. HCT116 and HEK293 cells (1×10^9 cells per well) were seeded in a 6-well plate and incubated at 37 °C humidified temperature with 5% CO_2 pressure for 24 h. Subsequently, the cells were treated with CNs–DOX (DOX conc. = 8.25 μg mL^{-1}), UCNs–DOX (DOX conc. = 6.62 μg mL^{-1}) and free DOX (conc. = 6.42 μg mL^{-1}) and they were further incubated for 24 h. Then the medium was discarded and the cells were washed 2 times with PBS. Finally, the cells were trypsinized, suspended in 500 μL PBS and transferred to a FACS tube for measuring the uptake of DOX by analyzing the fluorescence signal using flow cytometry.

Cell imaging by confocal laser scanning microscopy (CLSM). For imaging by Confocal Microscopy HCT116 & HEK293 cells (1×10^9 cells per well) were seeded in a 35 mm dish with a clean cover slip and incubated for 24 h. After reaching the desired confluency, the cells were treated with CNs–DOX, UCNs–DOX and free DOX (DOX concentration in each case = 8 μg mL^{-1}). After incubation for different time periods (3 h, 6 h, 12 h & 24 h) the cells were washed with PBS (phosphate buffered saline) twice and they were fixed by using 300 μL of 4% PFA (paraformaldehyde) for 5 minutes. After fixation, the cells were washed with PBS and the nuclei were stained with Hoechst 33342 for about 15 minutes. Then the cells were further washed 3 times with PBS and the cover slips were mounted on slides with 40% glycerol (sides of the cover slips were sealed with DPX) for imaging using CLSM.

Results and discussion

The acid-labile bolaamphiphilic molecule (BA) was synthesized in four steps using the thiol–acrylate Michael addition reaction as a key step. The self-assembly and container properties of BA were examined using a hydrophobic dye, Nile red as the fluorescence probe. Fig. S1† shows that the fluorescence intensity of Nile Red is very low at a low BA concentration, but increases with increasing BA concentration (Nile Red concentration is constant). This observation indicates that at a low concentration of BA, nanoassemblies were not formed, but with increasing concentration, more assemblies were formed, and Nile Red was encapsulated in the hydrophobic core of the nanoassemblies, which results in increased fluorescence intensity of Nile red. This experiment suggests the formation of nanoassemblies above a particular concentration of BA called critical aggregation concentration (CAC), and they are capable of sequestering hydrophobic guest molecules. From the inflection point of the plot in Fig. 1a, the CAC was found to be 0.6 mM. Another hydrophobic guest, pyrene, was also used to further confirm the container properties of the nanoassemblies. The pyrene molecule is very poorly soluble in water on its own, but in the presence of 1 mM BA solution, its solubility increased dramatically as shown by its emission spectrum (Fig. 1b). This can be attributed to the encapsulation of pyrene molecules in the core of the nanoassemblies. Since pyrene has a very distinct response to the polarity of its surrounding environment, we utilized the emission spectrum of encapsulated pyrene to determine the hydrophobicity of the core of the nanoassemblies. The hydrophobicity of the microenvironment can

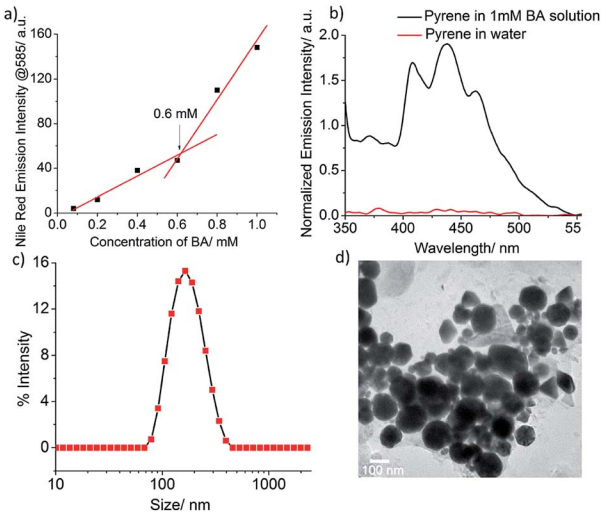

Fig. 1 Characterization of the self-assembled nanostructure of BA. (a) CAC determination using Nile red as a fluorescence probe, (b) pyrene encapsulation study, (c) DLS and (d) TEM image of self-assembled BA.

be calculated using the ratio of the first and third vibrational peaks (I_1/I_3, where I_1 = intensity at 373 nm and I_3 = intensity at 384 nm) of the emission spectrum of pyrene. Here, the I_1/I_3 value was found to be 1.09, which closely matched with the value of chlorobenzene (1.08), thus indicating that the dielectric constant of the core of the nanoassemblies is similar to that of chlorobenzene ($5.62\varepsilon_0$ at 20 °C).[63]

The formation of amphiphilic aggregates of BA in an aqueous milieu with an average hydrodynamic diameter of 160 nm was confirmed by dynamic light scattering (DLS) (Fig. 1c). The high-resolution transmission electron microscopy (TEM) analysis showed the presence of spherical nanoassemblies with sizes in the range of 130–140 nm (Fig. 1d), which are slightly lower than the value obtained from DLS. This is possibly due to the shrinkage of the particles in the dry state[64,65] or because of overestimation of the particle size in DLS, as here the average size is measured by taking into account the hydration shells around the particles. The morphology was further supported by atomic force microscopy images (AFM), which showed near-spherical nanostructures with the average height and width in the range of 6–16 nm and 100–120 nm, respectively (Fig. S2†).

Next, we hypothesized that cross-linked nanoassemblies would be stable in a large volume of solvent or blood serum and also at the same time they will stabilize the encapsulated guest molecules for a long time. To test this hypothesis, we cross-linked the micellar assembly by introducing 1,6-hexanedithiol into the hydrophobic core of the nanoassemblies followed by cross-linking the acrylate unit of BA using the thiol–acrylate Michael addition reaction with *n*-hexylamine as the catalyst. The ^{1}H NMR spectrum of the cross-linked nanoassemblies is presented in Fig. S3,† which shows the absence of the signal at δ 5.78–6.40 for the acrylate double bond and the appearance of the signal at δ 1.65 for $-CH_2$ protons of 1,6-hexanedithiol. This indicates the formation of the cross-linked nanoassemblies. The cross-linking reaction is presented in Fig. S4.† The dynamic

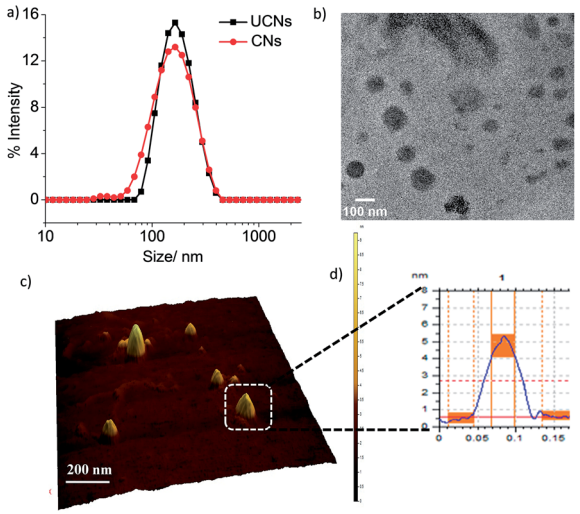

Fig. 2 Characterization of cross-linked nanoassemblies. (a) Comparison of the size of cross-linked (CNs) and uncross-linked (UCNs) nanoassemblies measured by DLS, (b and c) TEM image and AFM images of CNs, and (d) AFM height profile.

light scattering measurements showed that the hydrodynamic diameter of the nanoassemblies remains unchanged after cross-linking (Fig. 2a). This result suggests that a particular size of the CNs can be achieved by controlling the size of the preformed amphiphilic nanoassemblies by varying the concentration of monomers. The fact of precise size control of the nanoassemblies was further confirmed using TEM and AFM images (Fig. 2b–d) which showed spherical particles of 110–130 nm and 80–100 nm size respectively.

Next, we tested whether the CNs can maintain their size during dilution and also in serum. It is seen in Fig. 3a that the dilution did not affect the size of the CNs even though the concentration was below the CAC of BA. Since the CNs are expected to be administered intravenously for final applications, we were curious to see their stability in 10% FBS (fetal bovine serum). Fig. 3b shows that the CNs are stable even after 6 h of incubation at 10% FBS, while the uncross-linked nanoassemblies (UCNs) are disassembled under identical conditions, indicating the tolerance of CNs in the complex bloodstream. Hence, the DLS experiments in water and FBS revealed that the stability of the CNs is enhanced dramatically compared to that of UCNs.

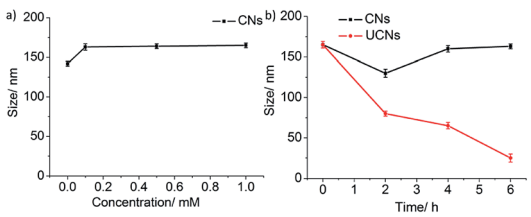

Fig. 3 *In vitro* stability of nanoassemblies in water and FBS. (a) Size of CNs as a function of concentration of BA in water. (b) Size change monitoring of CNs and UCNs in 10% FBS at 37 °C. Concentration of BA in both cases is 1 mM.

After the successful fabrication and characterization of CNs, we were curious to examine the possibility of pH-responsive noncovalent guest release by cleavage of the β-thioester linker at pH 5.3. At first, the pyrene molecules were encapsulated in the core of the nanoassemblies followed by cross-linking using dithiol to generate CNs with multiple copies of β-thioester groups in the core. Next, pyrene loaded CNs and UCNs were treated with Tris buffer of pH either 5.3 or 7.4 (buffer concentration = 10 mM) and absorption spectra of pyrene at 338 nm were monitored for 35 h for the quantification of the pyrene release kinetics. As shown in Fig. 4a and S4,† at neutral pH, the pyrene release rate was much slower (19% for CNs and 80% for UCNs within 35 h) in the case of CNs compared to UCNs, suggesting that the encapsulated guest leakage was significantly minimized due to cross-linked network formation. In contrast, at pH 5.3, an accelerated guest release was observed for CNs, but both the release rate and amount of guest released after 35 h were lower compared to those of UCNs, which indicates the capability of CNs for guest release in a controlled and sustained manner. This experiment concludes in favour of high guest encapsulation stability and controlled release capability of cross-linked nanoassemblies at endosomal relevant pH 5.3. Hence, considering the promising result obtained in *in vitro* dye release, we were interested in testing the potential of this cross-linked nanoassembly for chemotherapeutic delivery. To this end, we encapsulated an anti-cancer drug, doxorubicin, studied time-dependent pH-responsive *in vitro* release and examined anti-cancer activity using human colon cancer cells, HCT116. Dialysis was used to evaluate the pH-responsive release of DOX at pH 5.3 and pH 7.4. As shown in Fig. 4b, the DOX released after 24 h at neutral pH from CNs–DOX was ~21%, while for UCNs–DOX the value was ~41%, suggesting the significant minimization of leakage of encapsulated DOX due to cross-linking. Notably, upon adjusting the pH to 5.3, the DOX released from both CNs–DOX and UCNs–DOX after 24 h was increased to ~46% and 49% respectively. The slightly low release rate of CNs–DOX can be attributed to the cross-linked core of the nanoassemblies. The experimental conditions for the pH-responsive drug release mimicked the environment inside the endosomes (*i.e.*, pH ~ 5.5),[66–68] which suggests that the CNs have the potential for chemotherapeutic applications.

As it is very crucial to know the cytotoxicity of a drug carrier itself, we have carried out *in vitro* cell viability assays for empty

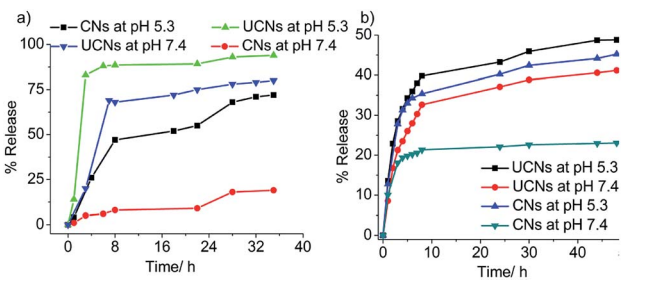

Fig. 4 Study of pH triggered *in vitro* guest release from UCNs and CNs. (a) Time dependent % release of (a) pyrene and (b) DOX from UCNs and CNs at pH 7.4 and pH 5.3 (Tris buffer). Concentration of BA = 1 mM.

CNs and UCNs using normal cell lines such as human embryonic kidney cell lines (HEK-293) and peripheral blood mononuclear cells (PBMC). The cells were treated with different concentrations of nanoassemblies and incubated for 24 h. The cell viability was measured using MTT assay. As shown in Fig. 5a and b, the CNs exhibit high cell viability in both the cell lines. This makes CNs a potential system for selective biological applications. For ultimate therapeutic applications, it is essential to test the effect of DOX-loaded nanocarriers on normal cells. To test this, HEK-293 cells or PBMC cells were treated with DOX-loaded CNs (CNs–DOX) and UCNs (UCNs–DOX) and incubated for 24 h. Notably, CNs–DOX was found to be non-toxic to both the normal cells, whereas UCNs–DOX showed high cytotoxicity, which can be attributed to two facts: one is the leakage of DOX from UCNs followed by diffusion through the cell membrane and another is burst release of DOX in the cytosol (Fig. 5d and e). As the UCNs–DOX showed a very similar behaviour to free DOX (cell death more than 75% in both cases), we assumed that the major contribution of UCNs to the observed cytotoxicity has come from the burst release of drugs. The benign nature of empty and DOX-loaded CNs towards normal cells makes this system more promising in the field of therapeutic applications.

Finally, the viability of CNs–DOX and UCNs–DOX was examined towards colon cancer cell lines (HCT-116), and the extent of cell death was investigated after 24 h. As shown in Fig. 5f, CNs–DOX caused almost 78% cell death, which is slightly lower than the free DOX and UCNs–DOX. This is presumably caused by the delayed release of DOX from the cross-linked nanoassemblies in the cell cytosol, while free DOX molecules easily diffuse through the cell membrane.[69] This phenomenon supports the higher IC_{50} value of CNs–DOX (8.25 μg mL^{-1}) and very similar IC_{50} values of UCNs–DOX and free DOX (6.60 μg mL^{-1} and 6.42 μg mL^{-1} respectively) (Fig. S5, Table S1†). As both the empty nanoassemblies (CNs and UCNs) showed very high cell viability towards HCT-116 cells (Fig. 5c), the cytotoxicity observed after treatment with DOX-loaded nanoassemblies was indeed caused by the released DOX molecules. The similarity in anti-cancer activity between UCNs–DOX and free DOX again strengthens the claim of partial leakage and majority burst release of drugs from UCNs. To get more insight into the drug delivery activity, the cellular internalization of CNs–DOX, UCNs–DOX, and free DOX was studied in HEK-293 cells and HCT-116 cells by FACS (fluorescence-activated cell sorting) assay and confocal microscopy. The FACS histograms are depicted in Fig. 6a and S6,† which demonstrate that CNs–DOX has almost no cellular internalization in HEK-293 cells, while in the case of HCT-116 cells, a significant increase in cellular uptake was observed, which explains the reason behind the benign nature of CNs–DOX towards HEK-293 cells. Hence, CNs–DOX exhibits very low cytotoxicity towards HEK-293 cells as there was no cellular uptake as observed in the FACS result and no DOX leakage due to the cross-linked core. The observed cell-specific viability can be supported very well by the FACS results. To get supporting data about cell-specific internalization, zeta potential measurements at different pH values (7.4 and 6.8) were performed. They revealed very important information about the surface charge of CNs–DOX and UCNs–DOX. The zeta potential of CNs–DOX and UCNs–DOX at pH 7.4 is found to be −0.2 mV and +10.0 mV respectively while at pH 6.8, it is +2.2 mV and +6.5 mV respectively (Fig. 6b). The negative zeta potential of CNs–DOX at pH 7.4 might be the reason for no

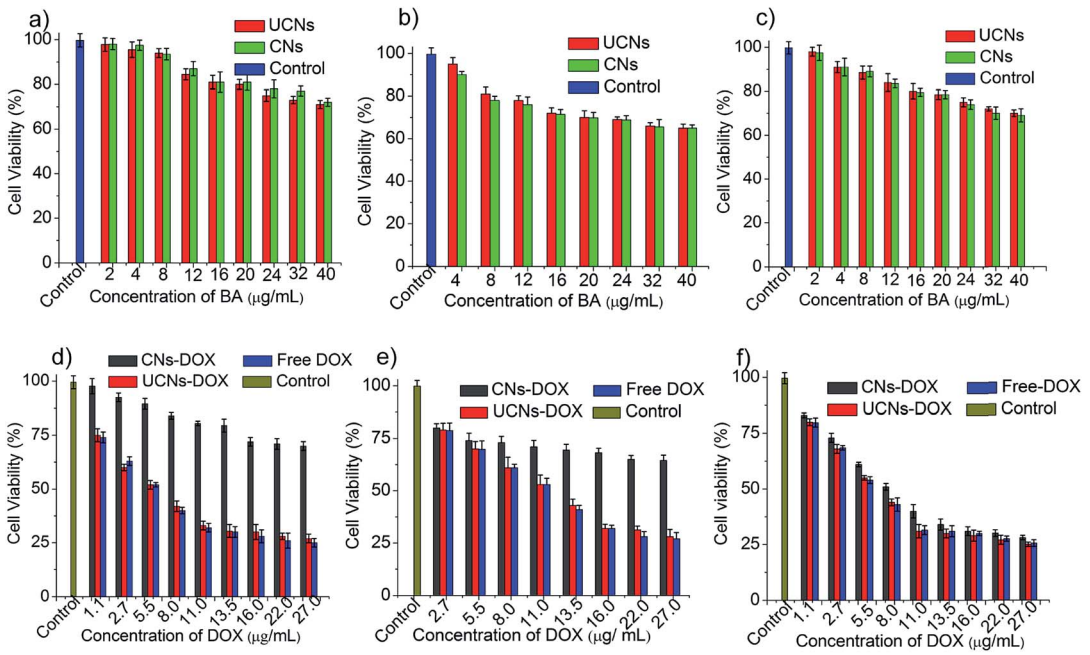

Fig. 5 *In vitro* cytotoxicity of empty and DOX loaded nanoassemblies by MTT assay. Incubated for 24 h with 5% CO_2 at 37 °C temperature. Top: Cell viability of empty CNs and UCNs against (a) HEK-293 cells, (b) PBMC and (c) HCT-116. Bottom: Dose responsive cell viability of CNs–DOX, UCNs–DOX and free DOX against (d) HEK-293 cells, (e) PBMC and (f) HCT-116 cells.

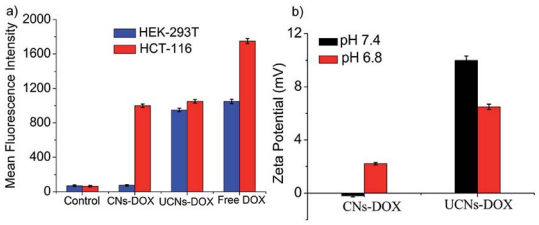

Fig. 6 Experiments supporting cell specificity. (a) Plot of mean fluorescence intensity observed from flow cytometry analysis representing the cellular uptake of DOX loaded nanoassemblies and free DOX in HEK-293 and HCT-116 cells. Incubation time = 24 h and temperature = 37 °C. (b) Zeta potential measurement of DOX loaded nanoassemblies at neutral and slightly acidic pH.

cellular internalization in normal cells. On the other hand, as the cancer cell environment is slightly acidic, at pH 6.8 both the DOX-loaded nanoassemblies showed a positive surface charge and accelerated cellular internalization. To strengthen the claim of opposite behaviour of CNs–DOX towards normal cells and cancer cells we performed an experiment, where the effect can be visualized by using a confocal microscope. The progress of the cellular internalization in HEK-293 cells and HCT-116 cells was monitored, and confocal images were taken at 3 h, 6 h, 12 h and 24 h time points, as shown in Fig. 7. Both free DOX and UCNs–DOX showed increased fluorescence intensity in a time-dependent manner for both the cell lines. On the other hand, CNs–DOX did not show any red colour (fluorescence colour of DOX) for HEK-293 cells, which suggests no cellular uptake, but interestingly showed time-dependent cellular uptake in HCT-116 cells. In this case, the fluorescence signals were less intense compared to those of free DOX and UNCs–DOX at every identical incubation time. This variation can be attributed to the difference in the cellular uptake mechanism. The free DOX enters the cell through diffusion and DOX in UCNs leaks out of the nanoassemblies due to less encapsulation stability and diffuses through the membrane. On the other hand, DOX in CNs is very stable, and the cells internalized the nanoassemblies along with the DOX by endocytosis, which is a slower process than the diffusion of a small molecule.

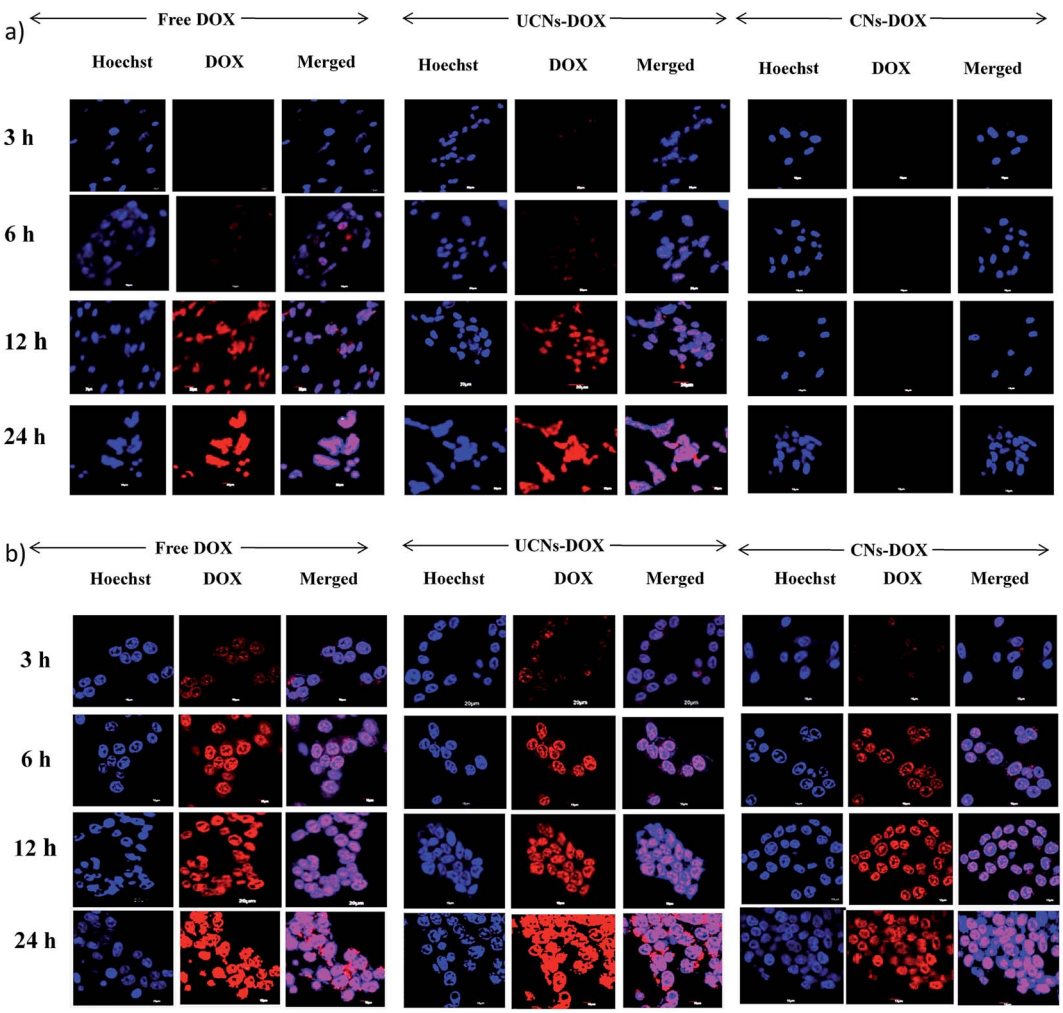

Fig. 7 CLSM images of (a) HEK-293 and (b) HCT-116 cells treated with free DOX, UCNs–DOX and CNs–DOX. Images were taken at incubation time points of 3 h, 6 h, 12 h and 24 h. In each panel left images show nuclei stained with Hoechst, middle images show the fluorescence of DOX in the cells and right images show the overlay of the previous two images. The scale bars are 20 μm in all images. Concentration of DOX in each case is 8 μg mL^{-1}.

Conclusions

In summary, we have designed and fabricated bolaamphiphile based cross-linked nanoassemblies (CNs) integrated with an acid labile functionality, β-thioester, which hydrolyses at acidic pH and leads the decross-linking of the nanoassemblies. Since the bolaamphiphile is a small molecule, it showed very high nanoassembly fabrication reproducibility and a high degree of control over their polydispersity and size, which are the major limitations of polymeric materials. As the core of the nanoassemblies is cross-linked, dilution induced disassembly was not observed even below the CAC of uncross-linked nanoassemblies. The CNs were also found to show good tolerance in serum compared to UCNs. Next, we noted that the environment specific (acidic pH) decross-linking caused the nanoassemblies to release the encapsulated guest molecules. To test cell microenvironment responsive drug release, we used the anticancer drug-loaded CNs and performed a few biological experiments, where we observed a distinct selectivity nature of CNs–DOX for cellular internalization and cytotoxicity towards cancer cells over normal cells. The DOX-loaded CNs were found to be nontoxic to HEK-293 and PBMC cells, but cytotoxic to HCT-116 cells. This excellent cell specificity of the cross-linked nanoassemblies is very fascinating and makes the system very interesting for further study to understand the detailed selectivity mechanism followed by *in vivo* applications using a mouse model. Therefore, as a concluding remark we can say that a few crucial features such as (i) fabrication reproducibility, (ii) robust serum stability, (iii) high guest encapsulation stability, (iv) pH-triggered drug release, (v) low toxicity of nanoassemblies itself, (vi) cancer cell-specific cytotoxicity, *etc.*, make this small molecule-based system a very promising potential candidate in the field of chemotherapeutic applications.

Conflicts of interest

There are no conflicts to declare.

Acknowledgements

We are thankful to the University of Calcutta (CU) for partial financial support, infrastructure, and instrumental facilities. We thank CRNN, CU for TEM facilities. We thank Dr Chittaranjan Sinha from Jadavpur University and Dr R. Natarajan and Dr Krishnananda Chattopadhyay from CSIR-IICB for allowing us to use the UV-Vis spectrometer, Fluorescence spectrometer, and DLS respectively. We thank Prof. Samit Chattopadhyay, Director of CSIR-IICB, Kolkata for giving us the opportunity to use the biological facilities of the institute. We also thank Mr Hayder Ali from IACS, Kolkata for helping us with the zeta potential measurements. We thank Prof. Dilip Kumar Maiti from the University of Calcutta for allowing us to use the DLS instrument in his lab. MRM thanks UGC, India for funding (Award number: F.30-426/2018 (BSR)), MS thanks DST, and SS, MAK thanks CSIR for their research fellowship.

References

1 J. Zhuang, M. R. Gordon, J. Ventura, L. Li and S. Thayumanavan, Multi-Stimuli Responsive Macromolecules and Their Assemblies, *Chem. Soc. Rev.*, 2013, **42**, 7421–7435.
2 S. M. Lee and S. T. Nguyen, Smart Nanoscale Drug Delivery Platforms from Stimuli-Responsive Polymers and Liposomes, *Macromolecules*, 2013, **46**, 9169–9180.
3 X. Hu, Y. Zhang, Z. Xie, X. Jing, A. Bellotti and Z. Gu, Stimuli-Responsive Polymersomes for Biomedical Applications, *Biomacromolecules*, 2017, **18**, 649–673.
4 A. P. Blum, J. K. Kammeyer, A. M. Rush, C. E. Callmann, M. E. Hahn and N. C. Gianneschi, Stimuli-Responsive Nanomaterials for Biomedical Applications, *J. Am. Chem. Soc.*, 2015, **137**, 2140–2154.
5 G. Han, T. Mokari, C. A. Franklin and B. E. Cohen, Caged Quantum Dots, *J. Am. Chem. Soc.*, 2008, **130**, 15811–15813.
6 G. Han, C. C. You, B. J. Kim, R. S. Turingan, N. S. Forbes, C. T. Martin and V. M. Rotello, Light-Regulated Release of DNA and Its Delivery to Nuclei by Means of Photolabile Gold Nanoparticles, *Angew. Chem., Int. Ed.*, 2006, **45**, 3165–3169.
7 Y. L. Zhao, Z. Li, S. Kabehie, Y. Y. Botros, J. F. Stoddart and J. I. Zink, pH-Operated Nanopistons on the Surfaces of Mesoporous Silica Nanoparticles, *J. Am. Chem. Soc.*, 2010, **132**, 13016–13025.
8 E. Climent, A. Bernardos, R. M. Manez, A. Maquieira, M. D. Marcos, N. P. Navarro, R. Puchades, F. Sancenon, J. Soto and P. Amoros, Controlled Delivery Systems Using Antibody-Capped Mesoporous Nanocontainers, *J. Am. Chem. Soc.*, 2009, **131**, 14075–14080.
9 M. R. Molla, A. Böser, A. Rana, K. Schwarz and P. A. Levkin, One-Pot Parallel Synthesis of Lipid Library *via* Thiolactone Ring Opening and Screening for Gene Delivery, *Bioconjugate Chem.*, 2018, **29**, 992–999.
10 E. G. Kelley, J. N. L. Albert, M. O. Sullivan and T. H. Epps, Stimuli-Responsive Copolymer Solution and Surface Assemblies for Biomedical Applications, *Chem. Soc. Rev.*, 2013, **42**, 7057–7071.
11 F. D. Jochumab and P. Theato, Temperature- and Light-Responsive Smart Polymer Materials, *Chem. Soc. Rev.*, 2013, **42**, 7468–7483.
12 S. Zhang, Y. Wu, B. He, K. Luo and Z. Gu, Biodegradable Polymeric Nanoparticles Based on Amphiphilic Principle: Construction and Application in Drug Delivery, *Sci. China: Chem.*, 2014, **57**, 461–475.
13 R. Aluri and M. Jayakannan, Development of L-Tyrosine-Based Enzyme-Responsive Amphiphilic Poly(ester-urethane) Nanocarriers for Multiple Drug Delivery to Cancer Cells, *Biomacromolecules*, 2017, **18**, 189–200.
14 A. W. Bosman, H. M. Janssen and E. W. Meijer, About Dendrimers: Structure, Physical Properties, and Applications, *Chem. Rev.*, 1999, **99**, 1665–1688.
15 S. M. Grayson and J. M. J. Fréchet, Convergent Dendrons and Dendrimers: From Synthesis to Applications, *Chem. Rev.*, 2001, **101**, 3819–3867.

16 M. Fischer and F. Vögtle, Dendrimers: From Design to Application – A Progress Report, *Angew. Chem., Int. Ed.*, 1999, **38**, 884–905.
17 S. Svenson and D. A. Tomalia, Dendrimers in Biomedical Applications—Reflections on the Field, *Adv. Drug Delivery Rev.*, 2005, **57**, 2106–2129.
18 D. A. Tomalia and J. M. J. Fréchet, Discover of Dendrimers and Dendritic Polymers: A Brief Historical Perspective, *J. Polym. Sci. A*, 2002, **40**, 2719–2728.
19 A. R. Menjoge, R. M. Kannan and D. A. Tomalia, Dendrimer-Based Drug and Imaging Conjugates: Design Considerations for Nanomedical Applications, *Drug Discovery Today*, 2010, **15**, 171–185.
20 B. M. Rosen, C. J. Wilson, D. A. Wilson, M. Peterca, M. R. Imam and V. Percec, Dendron-Mediated Self-Assembly, Disassembly, and Self-Organization of Complex Systems, *Chem. Rev.*, 2009, **109**, 6275–6540.
21 V. Percec, D. A. Wilson, P. Leowanawat, C. J. Wilson, A. D. Hughes, M. S. Kaucher, D. A. Hammer, D. H. Levine, A. J. Kim, F. S. Bates, K. P. Davis, T. P. Lodge, M. L. Klein, R. H. DeVane, E. Aqad, B. M. Rosen, A. O. Argintaru, M. J. Sien-kowska, K. Rissanen, S. Nummelin and J. Ropponen, Self-Assembly of Janus Dendrimers into Uniform Dendrimersomes and Other Complex Architectures, *Science*, 2010, **328**, 1009–1014.
22 D. Joester, M. Losson, R. Pugin, H. Heinzelmann, E. Walter, H. P. Merkle and F. Diederich, Amphiphilic Dendrimers: Novel Self-Assembling Vector for Efficient Gene Delivery, *Angew. Chem., Int. Ed.*, 2003, **42**, 1486–1490.
23 A. I. Cooper, J. D. Londono, G. Wig-nall, J. B. McClain, E. T. Samulski, J. S. Lin, A. Dobrynin, M. Rubinstein, A. L. C. Burke, J. M. J. Fréchet and J. M. DeSimone, Extraction of a Hydrophilic Compound from Water into Liquid CO_2 using Dendritic Surfactant, *Nature*, 1997, **389**, 368–371.
24 G. R. Newkome, C. N. Moore-field, G. R. Baker, A. L. Johnson and R. K. Behera, Alkane Cascade Polymers Possessing Micellar Topology: Micellanoic Acid Derivatives, *Angew. Chem., Int. Ed.*, 1991, **30**, 1176–1178.
25 C. J. Hawker, K. L. Wooley and J. M. J. Fréchet, Unimolecular Micelles and Globular Amphiphiles: Dendritic Macromolecules as Novel Recyclable Solubilization Agents, *J. Chem. Soc., Perkin Trans. 1*, 1993, 1287–1297.
26 Y. Wang, N. Ma, Z. Wang and X. Zhang, Photocontrolled Reversible Supramolecular Assemblies of an Azobenzene-Containing Surfactant with α-Cyclodextrin, *Angew. Chem., Int. Ed.*, 2007, **46**, 2823–2826.
27 Y. Orihara, A. Matsumura, Y. Saito, N. Ogawa, T. Saji, A. Yama-guchi, H. Sakai and M. Abe, Reversible Release Control of an Oily Substance Using Photoresponsive Micelles, *Langmuir*, 2001, **17**, 6072–6076.
28 K. Dan, R. Pan and S. Ghosh, Aggregation and pH Responsive Disassembly of a New Acid-Labile Surfactant Synthesized by Thiol–Acrylate Michael Addition Reaction, *Langmuir*, 2011, **27**, 612–617.
29 M. R. Molla and S. Ghosh, Hydrogen-Bonding-Mediated Vesicular Assembly of Functionalized Naphthalene-Diimide-Based Bolaamphiphile and Guest-Induced Gelation in Water, *Chem.–Eur. J.*, 2012, **18**, 9860–9869.
30 P. Xing and Y. Zhao, Multifunctional Nanoparticles Self-Assembled from Small Organic Building Blocks for Biomedicine, *Adv. Mater.*, 2016, **28**, 7304–7339.
31 P. Pramanik, D. Halder, S. S. Jana and S. Ghosh, pH-Triggered Sustained Drug Delivery from a Polymer Micelle having the Thiopropionate Linkage, *Macromol. Rapid Commun.*, 2016, **37**, 1499–1506.
32 S. Mukherjee, H. Dinda, I. Chakraborty, R. Bhattacharyya, J. D. Sarma and R. Shunmugam, Engineering Camptothecin-Derived Norbornene Polymers for Theranostic Application, *ACS Omega*, 2017, **2**, 2848–2857.
33 B. Surnar and M. Jayakannan, Structural Engineering of Biodegradable PCL Block Copolymer Nanoassemblies for Enzyme-Controlled Drug Delivery in Cancer Cells, *ACS Biomater. Sci. Eng.*, 2016, **2**, 1926–1941.
34 M. R. Molla, P. Rangadurai, G. M. Pavan and S. Thayumanavan, Experimental and Theoretical Investigations in Stimuli Responsive Dendrimer-based Assemblies, *Nanoscale*, 2015, **7**, 3817–3837.
35 L. Li, Z. Bai and P. A. Levkin, Boronate-dextran: An Acid-Responsive Biodegradable Polymer for Drug Delivery, *Biomaterials*, 2013, **34**, 8504–8510.
36 S. R. Mane, V. Rao, K. Chaterjee, H. Dinda, S. Nag, A. Kishore, J. D. Sarma and R. Shunmugam, Amphiphilic Homopolymer Vesicles as Unique Nano-Carriers for Cancer Therapy, *Macromolecules*, 2012, **45**, 8037–8042.
37 N. U. Deshpande and M. Jayakannan, Cisplatin-Stitched Polysaccharide Vesicles for Synergistic Cancer Therapy of Triple Antagonistic Drugs, *Biomacromolecules*, 2017, **18**, 113–126.
38 K. Dan and S. Ghosh, One-Pot Synthesis of an Acid-Labile Amphiphilic Triblock Copolymer and its pH-Responsive Vesicular Assembly, *Angew. Chem., Int. Ed.*, 2013, **52**, 7300–7305.
39 M. R. Molla, P. Rangadurai, L. Antony, S. Swaminathan, J. J. de Pablo and S. Thayumanavan, Dynamic Actuation of Glassy Polymersomes Through Isomerization of a Single Azobenzene Unit at the Block Copolymer Interface, *Nat. Chem.*, 2018, **10**, 659–666.
40 A. Saha, S. Mohapatra, G. Das, B. Jana, S. Ghosh, D. Bhunia and S. Ghosh, Cancer Cell Specific Delivery of Photosystem I through Integrin Targeted Liposome Shows Significant Anticancer Activity, *ACS Appl. Mater. Interfaces*, 2017, **9**, 176–188.
41 T. M. Allen and P. R. Cullis, Liposomal Drug Delivery Systems: From Concept to Clinical Applications, *Adv. Drug Delivery Rev.*, 2013, **65**, 36–48.
42 R. Gui, A. Wan, X. Liu and H. Jina, Intracellular Fluorescent Thermometry and Photothermal-Triggered Drug Release Developed from Gold Nanoclusters and Doxorubicin Dual-Loaded Liposomes, *Chem. Commun.*, 2014, **50**, 1546–1548.
43 S. Mura, J. Nicolas and P. Couvreur, Stimuli-Responsive Nanocarriers for Drug Delivery, *Nat. Mater.*, 2013, **12**, 991–1003.

44 C. Liao, Y. Chen, Y. Yao, S. Zhang, Z. Gu and X. Yu, Cross-Linked Small-Molecule Micelle-Based Drug Delivery System: Concept, Synthesis, and Biological Evaluation, *Chem. Mater.*, 2016, **28**, 7757–7764.

45 Y. Chen, J. Huang, S. Zhang and Z. Gu, Superamphiphile Based Cross-Linked Small-Molecule Micelles for pH-Triggered Release of Anticancer Drugs, *Chem. Mater.*, 2017, **29**, 3083–3091.

46 G. Chadha, Q. Z. Yang and Y. Zhao, Self-Assembled Light-Harvesting Supercomplexes from Fluorescent Surface-Cross-Linked Micelles, *Chem. Commun.*, 2015, **51**, 12939–12942.

47 Y. Shao, C. Shi, G. Xu, D. Guo and J. Luo, Photo and Redox Dual Responsive Reversibly Cross-Linked Nanocarrier for Efficient Tumor-Targeted Drug Delivery, *ACS Appl. Mater. Interfaces*, 2014, **6**, 10381–10392.

48 J. Huang, F. Wu, Y. Yu, H. Huang, S. Zhang and J. You, Lipoic Acid Based Core Cross-Linked Micelles for Multivalent Platforms: Design, Synthesis and Application in Bio-Imaging and Drug Delivery, *Org. Biomol. Chem.*, 2017, **15**, 4798–4802.

49 Y. Shi, C. F. van Nostrum and W. E. Hennink, InterfaciallyHydrazone Cross-linked Thermosensitive Polymeric Micelles for Acid-Triggered Release of Paclitaxel, *ACS Biomater. Sci. Eng.*, 2015, **1**, 393–404.

50 M. R. Molla, T. Marcinko, P. Prasad, D. Deming, S. C. Garman and S. Thayumanavan, Unlocking a Caged Lysosomal Protein from a Polymeric Nanogel with a pH Trigger, *Biomacromolecules*, 2014, **15**, 4046–4053.

51 S. Jiwpanich, J. H. Ryu, S. Bickerton and S. Thayumanavan, Noncovalent Encapsulation Stabilities in Supramolecular Nanoassemblies, *J. Am. Chem. Soc.*, 2010, **132**, 10683–10685.

52 J. H. Ryu, S. Jiwpa-nich, R. Chacko, S. Bickerton and S. Thayumanavan, Surface-Functionalizable Polymer Nanogels with Facile Hydrophobic Guest Encapsulation Capabilities, *J. Am. Chem. Soc.*, 2010, **132**, 8246–8247.

53 J. He, Y. Xia, Y. Niu, D. Hu, X. Xia, Y. Lu and W. Xu, pH Responsive Core Crosslinked Polycarbonate Micelles *via* Thiol–Acrylate Michael addition Reaction, *J. Appl. Polym. Sci.*, 2016, **134**, 44421.

54 Z. Zhang, L. Yin, C. Tu, Z. Song, Y. Zhang, Y. Xu, R. Tong, Q. Zhou, J. Ren and J. Cheng, Redox-Responsive, Core Cross-Linked Polyester Micelles, *ACS Macro Lett.*, 2013, **2**, 40–44.

55 M. Oishi, Y. Nagasaki, K. Itaka, N. Nishiyama and K. Kataoka, Lactosylated Poly (ethylene glycol)–siRNA Conjugate through Acid-Labile β-Thiopropionate Linkage to Construct pH-Sensitive Polyion Complex Micelles Achieving Enhanced Gene Silencing in Hepatoma Cells, *J. Am. Chem. Soc.*, 2005, **127**, 1624–1625.

56 M. Oishi, S. Sa-saki, Y. Nagasaki and K. Kataoka, pH-Responsive Oligodeoxynucleotide (ODN)–Poly (Ethylene Glycol) Conjugate through Acid-Labile β-Thiopropionate Linkage: Preparation and Polyion Complex Micelle Formation, *Biomacromolecules*, 2003, **4**, 1426–1432.

57 S. Zhang and Y. Zhao, Rapid Release of Entrapped Contents from Multi-Functionalizable, Surface Cross-Linked Micelles upon Different Stimulation, *J. Am. Chem. Soc.*, 2010, **132**, 10642–10644.

58 Y. Rui, S. Wang, P. S. Low and D. H. Thompson, Diplasmenylcholine-Folate Liposomes: An Efficient Vehicle for Intracellular Drug Delivery, *J. Am. Chem. Soc.*, 1998, **120**, 11213–11218.

59 A. P. Goodwin, J. L. Mynar, Y. Ma, G. R. Fleming and J. M. J. Fréchet, Synthetic Micelle Sensitive to IR Light *via* a Two-Photon Process, *J. Am. Chem. Soc.*, 2005, **127**, 9952–9953.

60 D. A. Jaeger and Y. M. Sayed, Synthesis and characterization of single-chain second generation cleavable surfactants, *J. Org. Chem.*, 1993, **58**, 2619–2627.

61 D. Ono, A. Masuyama and M. Okahara, Preparation of New Acetal Type Cleavable Surfactants from Epichlorohydrin, *J. Org. Chem.*, 1990, **55**, 4461–4464.

62 D. A. Jaeger, J. Jamrozik, T. G. Golich, J. Clennan and M. W. Mohebalian, Preparation and Characterization of Glycerol-Based Cleavable Surfactants and Derived Vesicles, *J. Am. Chem. Soc.*, 1989, **111**, 3001–3006.

63 K. Kalyanasundaram and J. K. Thomas, Environmental Effects on Vibronic Band Intensities in Pyrene Monomer Fluorescence and Their Application in Studies of Micellar Systems, *J. Am. Chem. Soc.*, 1977, **99**, 2032–2039.

64 A. O. Moughton and R. K. O'Reilly, Thermally Induced Micelle to Vesicle Morphology Transition for a Charged Chain End Diblock Copolymer, *Chem. Commun.*, 2010, **46**, 1091–1093.

65 C. Qian, S. Zhang, J. Li, B. Zuo and X. Wang, Segmental Relaxation Behavior of Polystyrene Chains in the Cores of Collapsed Dry Micelles Tethered on the Micelle Film Surface by a Poly (Acrylic Acid) Corona, *Soft Matter*, 2014, **10**, 1579–1590.

66 G. Helmlinger, A. Sckell, M. Dellian, N. S. Forbes and R. K. Jain, Acid Production in Glycolysis-impaired Tumors Provides New Insights into Tumor Metabolism, *Clin. Cancer Res.*, 2002, **8**, 1284–1291.

67 A. S. Trevani, G. Andonegui, M. D. Giordano, H. López, R. Gamberale, F. Minucci and J. R. Geffner, Extracellular Acidification Induces Human Neutrophil Activation, *J. Immunol.*, 1999, **162**, 4849–4857.

68 K. Engin, D. B. Leeper, J. R. Cater, A. J. Thistlethwaite, L. Tupchong and J. D. Mcfarlane, Extracellular pH Distribution in Human Tumours, *Int. J. Hyperthermia*, 1995, **11**, 211–216.

69 X. W. Dai, Z. L. Yue, M. E. Eccleston, J. Swartling, N. K. H. Slater and C. F. Kaminski, Fluorescence Intensity and Lifetime Imaging of Free and Micellar-Encapsulated Doxorubicin in Living Cells, *Nanomedicine*, 2008, **4**, 49–56.

